J Mater Sci (2010) 45:4040–4045
DOI 10.1007/s10853-010-4486-4

Visible-light activities of $Gd_2O_3/BiVO_4$ composite photocatalysts

Aiping Zhang · Jinzhi Zhang

Received: 5 November 2009 / Accepted: 6 April 2010 / Published online: 22 April 2010

Abstract $Gd_2O_3/BiVO_4$ composite photocatalysts were hydrothermal synthesized and characterized by X-ray diffraction, X-ray photoelectron spectroscopy, scanning electron microscopy, and UV–vis diffusion reflectance spectra; all the composite photocatalysts exhibited enhanced photocatalytic activities than the pure $BiVO_4$ for degradation of methyl orange under visible-light irradiation. The improved activity of composites was discussed and ascribed to the electron-scavenging effect of dopants.

Introduction

Bismuth vanadate ($BiVO_4$), one of the non-titania based visible-light-driven photocatalyts [1, 2], has recently attracted considerable attentions as it is commonly used as a photocatalyst in water splitting and oxidative decomposition of organic contaminants under visible-light irradiation [3–5]. Yet, the photocatalytic activity of the pure $BiVO_4$ is not so strong due to its low quanta yield caused by the difficult migration of photogenerated electron-hole pairs [6–8]. As an efficient way to solve this problem, loading metal or metal oxide can always enhance the photocatalytic activities of catalysts via separating the photogenerated electrons from holes.

Recently, $Ag/BiVO_4$ composite, prepared by Kohtani et al. [9] through an aqueous medium technique, showed superior visible-light activities in decomposing long-chain alkylphenols and polycyclic aromatic hydrocarbons than that of pure $BiVO_4$. Long et al. [10] and Chatchai et al. [11] found that $Co_3O_4/BiVO_4$ composite photocatalyst exhibited enhanced photocatalytic activity than pure $BiVO_4$ under visible-light irradiation, individually. Xu et al. [12] reported that $CuO/BiVO_4$ catalyst exhibited improved photocatalytic activity for the degradation of methylene blue; and the similar result had also obtained by Jiang et al. [13]. Ge [14, 15] prepared $PdCl_4/BiVO_4$ by the impregnation method and demonstrated that it exhibited enhanced photocatalytic activities in decomposition of aqueous methyl orange (MO) under visible-light irradiation. Besides, other metal or metal oxide including Fe_2O_3 [7], MnO_2 [16], CeO_2 [17], WO_3 [11], MoO_3 [18], V_2O_5 [19], Bi_2O_3 [20] loaded on $BiVO_4$ surface had been demonstrated to be effective in improving the photocatalytic activities of $BiVO_4$.

Although there have been many reports on transition metal and noble metal doped on $BiVO_4$, the effect of rare earth element doping on the photocatalytic activity of $BiVO_4$ for the organic contaminants photodegradation has seldom been reported [21] and need further study. Meanwhile, some investigations showed that lanthanide ions/oxides with 4f electron configuration were better dopants on improving the activities of photocatalysts. El-Bahy et al. [22] and Xie et al. [23], respectively, reported that lanthanide ions can enhance the photocatalytic activity of TiO_2 for photodegradation of dyes under visible-light irradiation. In this work, $Gd_2O_3/BiVO_4$ composites were hydrothermal synthesized and characterized by XRD, XPS, SEM, and DRS techniques. The influence of Gd_2O_3 loading on the photocatalytic decolorization of MO under visible-light irradiation was studied and also discussed.

A. Zhang (✉) · J. Zhang
College of Sciences, North China University of Technology, Beijing 100144, People's Republic of China
e-mail: ncutalex@126.com

Experimental

Synthesis of gadolinium doped bismuth vanadate

In a typical preparation process [24], 0.02 mol $Bi(NO_3)_3 \cdot 5H_2O$ and 0.02 mol NH_4VO_3 were dissolved separately in 20 mL of a 35% (w/w) HNO_3 and 20 mL of a 6 mol/L NaOH solutions, and each stirred for 30 min at room temperature. After that, these two mixtures were mixed together in a 1:1 M ratio and stirred for about 30 min to get a stable, salmon pink homogeneous solution. The different amounts of $Gd(NO_3)_3$ (0.1, 0.2, 0.5, 1.0, and 2.0 g) were then added into these solutions individually with a continuing stirring for 30 min to get the precursors. Mixture of each precursor were then sealed in a 50 mL Teflon-lined stainless autoclave and heated to 180 °C for 6 h under autogenous pressure. Afterwards, the precipitate was filtered, washed with distilled water three times for each, and dried in vacuum at room temperature for 12 h.

Apparatus and measurements

X-ray powder diffraction patterns (XRD, Puxi Co. LTD, model XD-3) were recorded in the region of $2\theta = 10$–$55°$ using Cu Kα radiation ($\lambda = 0.15418$ nm) with a scan step of 2.0°/min using a counter diffractometer. The morphologies and microstructures of samples were examined with scanning electron microscopy (SEM, FEI, model Quanta-600). Energy dispersive spectroscopy (EDS) in the whole SEM picture was also taken for the chemical analysis of the dopant. The BET special surface area of the catalysts was measured by N_2 adsorption at 77 K using a surface area detector (Jinaipu Co. LTD, model F-Sorb2400). X-ray photoelectron spectroscopy (XPS) analysis was performed on an X-ray photoelectron spectrometer (VG LIMS, model MKII) using the Mg Kα radiation. Optical absorbance spectra were obtained using a doubled-beam UV–vis spectrophotometer (Puxi Co. LTD, model TU-1901) equipped with an integrating sphere. UV–vis diffuse reflectance spectra (DRS) were recorded using $BaSO_4$ as a reference and were converted from reflection to absorbance by Kubelka–Munk method.

Photocatalytic activity test

Photocatalytic activities of the catalysts were determined by the decolorization of MO under visible-light irradiation. A 500 W Xe-illuminator was used as a light source and set about 10 cm apart from the reactor. The 420 nm cutoff filter was placed between the Xe-illuminator and the reactor to completely remove all the incoming wavelengths shorter than 420 nm to provide visible-light irradiation ($\lambda > 420$ nm). Experiments were carried out at ambient temperature as follows: the same amount (0.2 g) of photocatalyst was added into 100 mL of a 10 mg/L MO solution. Before illumination, the solution was stirred for 30 min in darkness in order to reach the adsorption–desorption equilibrium for MO and dissolved oxygen. At different irradiation time intervals, about 5 mL suspensions were collected, centrifugalized to remove the photocatalyst particles, and then used for the absorption tests. The concentrations of the remnant MO were monitored in the way of checking the absorbance of solutions at 464 nm during the photodegradation process.

Results and discussion

SEM–EDS results of the catalysts

Figure 1 shows the SEM images of different catalysts, accompanying with their BET-surface-area data listed in Table 1. In Fig. 1a, pure $BiVO_4$ particles with an average size of about 1–2 μm sintered heavily to be large aggregates. Contrastly, $Gd_2O_3/BiVO_4$ composite particles dispersed to each other in Fig. 1b–d; and when the Gd content increased, large aggregates with edges and smooth surface were obtained, as can be seen in Fig. 1e and f. It signifies that the presence of $Gd(NO_3)_3$ in the precursor influenced the dispersion and morphologies of products, which may foreshow the improved activities of these composites. This is because the recombination between photogenerated electrons and holes can be suppressed on the edges of catalysts [9, 25, 26]. In addition, the experimental data of Gd content from EDS agree with the precursor amounts, as listed in Table 1.

XRD analysis

The composite photocatalysts with Gd content of 0.28, 0.71, 1.22, and 2.93 wt% have single monoclinic scheelite structures from their powder X-ray diffraction (XRD) patterns; and all the diffraction peaks of these catalysts are in conformity to the standard card of the monoclinic $BiVO_4$ (JCPDS card No: 14-0688), as can be seen from Fig. 2a–e. For the 5.74 wt% composite catalyst, some characteristic peaks ascribed to gadolinium oxide (Gd_2O_3, JCPDS card No: 42-1465) appeared in the XRD patterns along with those for the monoclinic $BiVO_4$ in Fig. 2f. This indicates that the 5.74 wt% composite catalyst is composed of monoclinic $BiVO_4$ and Gd_2O_3.

XPS studies

The survey XPS spectrum for 1.22 and 5.74 wt% composite photocatalyst were shown in Fig. 3. Five elements including Bi, V, O, C, and Gd were found in the catalysts, and the element C may come from the adsorbed carbon

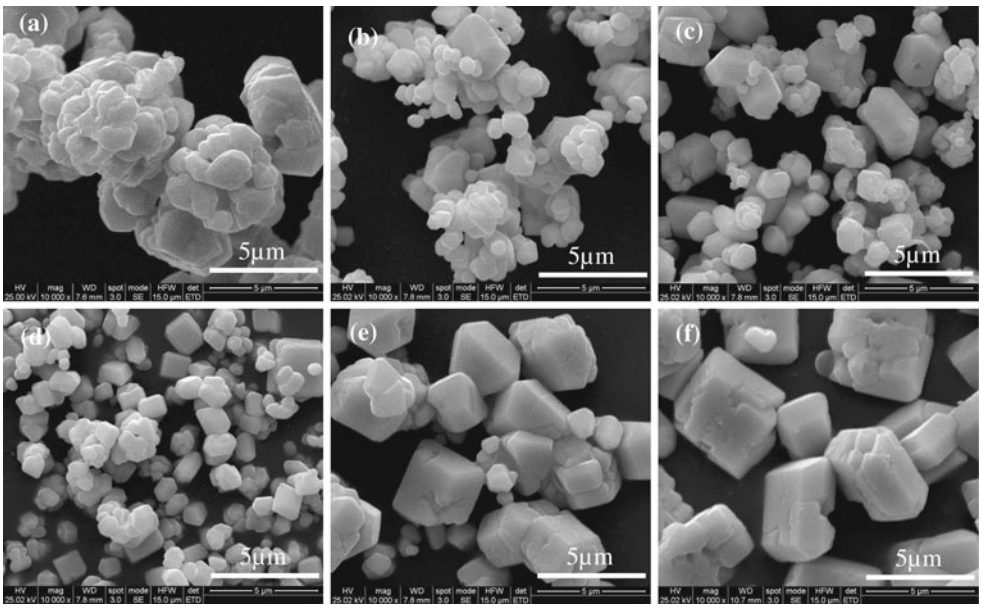

Fig. 1 SEM images of different catalysts: **a** pure $BiVO_4$, **b** 0.28 wt%, **c** 0.71 wt%, **d** 1.22 wt%, **e** 2.93 wt%, and **f** 5.74 wt% of Gd in composite

dioxide from air as others [12]. The high resolution XPS spectra of Bi4f, V2p, O1s, and Gd3d in composite catalyst were also observed in Fig. 4. Binding energy for Bi4f and V2p were centered at 159.4, 164.7, 517.2, and 524.0 eV, which are consistent with that of $Bi4f_{7/2}$, $Bi4f_{5/2}$, $V2p_{3/2}$, and $V2p_{1/2}$, respectively [11, 12]. The asymmetric XPS spectrum of O1s peak (Fig. 4c) indicates that different oxygen species exist on the surface of the composite photocatalyst. The binding energy located at 532.9 and 530.3 eV ascribe separately to the O1s orbit of lattice oxygen of Gd_2O_3 crystallites [27, 28] and $BiVO_4$ crystallites [12, 15]. The determined $Gd3d_{5/2}$ and $Gd3d_{3/2}$ binding energy at 1188.7 and 1218.6 eV were also consistent with those of Gd in the form of Gd_2O_3 [28, 29].

Kubelka–Munck transformed DRS of the photocatalysts

Figure 5 depicts the Kubelka–Munck transformed DRS of the pure $BiVO_4$ and $Gd_2O_3/BiVO_4$ composite catalysts. It

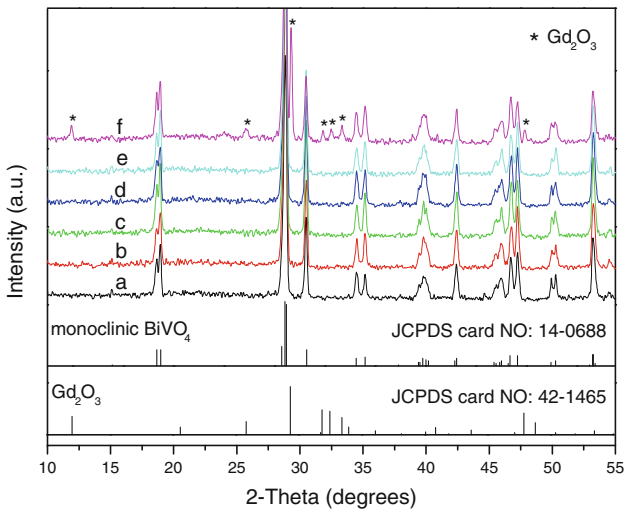

Fig. 2 XRD patterns of different catalysts: (*a*) pure $BiVO_4$, (*b*) 0.28 wt%, (*c*) 0.71 wt%, (*d*) 1.22 wt%, (*e*) 2.93 wt%, and (*f*) 5.74 wt% of Gd in composite

Table 1 Comparison of the parameters and photocatalytic ability for the catalysts

Catalyst (Gd content, wt%)		A_{BET} ($m^2\ g^{-1}$)	The first order kinetic equation (t, min)	Degradation rate, D% (3.5 h)
Precursor amount	EDS result			
0.00	0.00	1.93	$\ln(C_0/C_t) = 0.0011t + 0.0141$	13.75
0.37	0.28	2.68	$\ln(C_0/C_t) = 0.2187t + 0.0271$	47.90
0.74	0.71	2.96	$\ln(C_0/C_t) = 0.2559t + 0.0382$	54.83
1.49	1.22	3.59	$\ln(C_0/C_t) = 0.4701t + 0.0486$	87.94
3.72	2.93	2.55	$\ln(C_0/C_t) = 0.3238t + 0.2029$	72.66
7.43	5.74	1.89	$\ln(C_0/C_t) = 0.2109t + 0.0296$	46.25

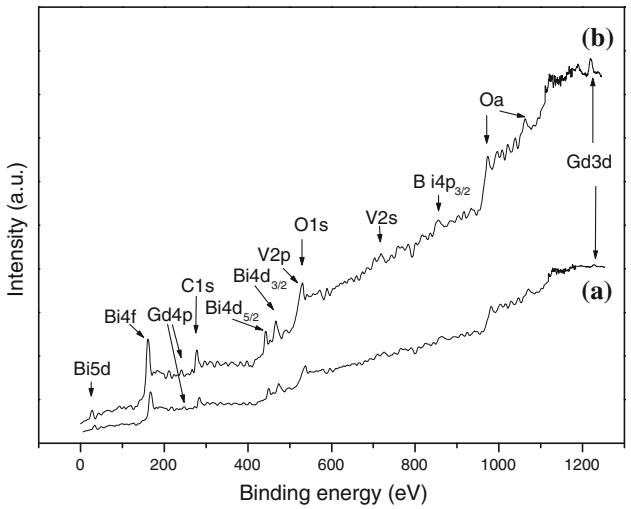

Fig. 3 XPS spectrum of (*a*) 1.22 wt% and (*b*) 5.74 wt% Gd in composite

is clear that the absorption edge of the composite catalysts extended a gradually red shift, and the absorbance intensity in the visible range also increased step by step with the increase of Gd content. The charge transfer between earth-metallic ion and semiconductor always leads to the shift of absorption edges [30, 31]; furthermore, surface area, morphology, and microstructure properties changes of composites may also cause the edge shift in DRS spectra. Since the yield of the photogenerated electron-hole pair may depend on the absorbance intensity and the absorption region with energy exceeding or equaling to the photocatalyst band-gap energy, it may indicate that the composite catalysts should exhibit enhanced photocatalytic activities than pure $BiVO_4$ from their DRS results.

Photocatalytic activities

The absorption spectra changes of MO aqueous solution at different irradiation time during the photodegradation process were shown in the inset of Fig. 6; and the decrease of absorption intensity at $\lambda_{max} = 465$ nm in these figures indicates the degradation of MO molecules. For pure $BiVO_4$ (inset of Fig. 6a), the absorbance of MO at 465 nm decreased a little after 3.5 h irradiation, suggesting that only the tiny part of the MO molecules in the solution had been decomposed. In contrast, the absorbance at 465 nm decreased much faster at the same time scale for the MO solutions using $Gd_2O_3/BiVO_4$ composite catalysts. However, the degradation rate of MO did not increase further after the turning content (about 1.22 wt%), but had a decrease trend with the further increase of Gd content, as can be seen from the inset of Fig. 6d–f.

Most of the heterogeneous photocatalytic degradation reactions follow Langmuir–Hinshelwood kinetic [32]

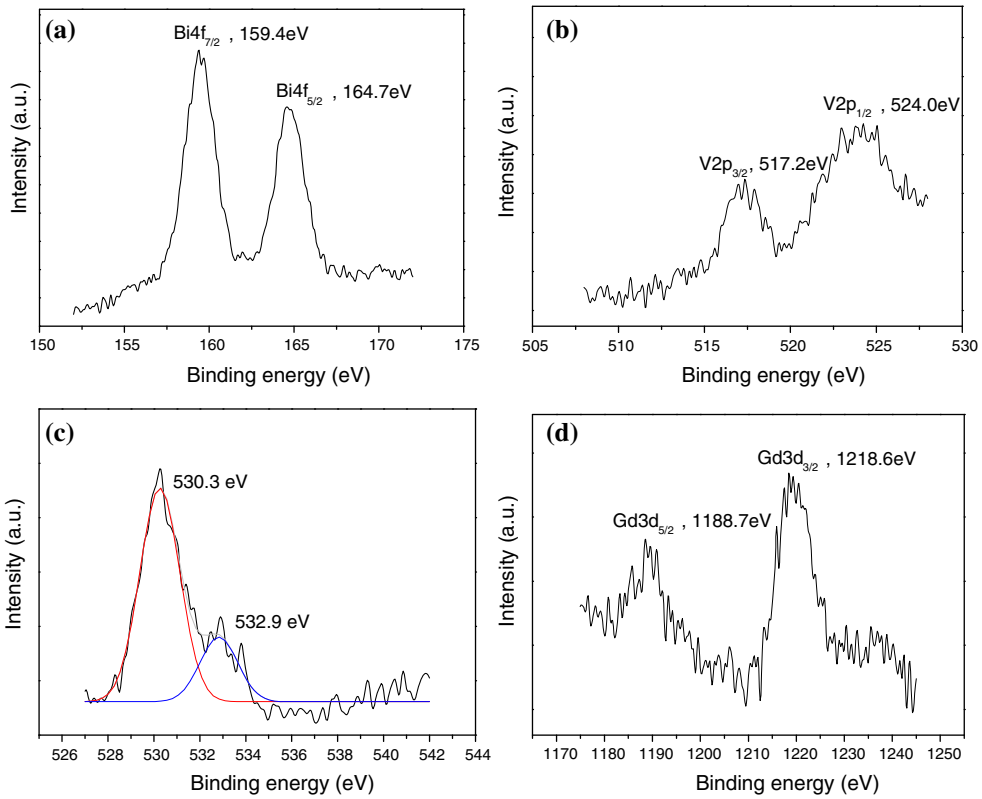

Fig. 4 XPS analysis of 5.74 wt% of Gd in composite: **a** Bi4f, **b** V2p, **c** O1s, and **d** Gd3d

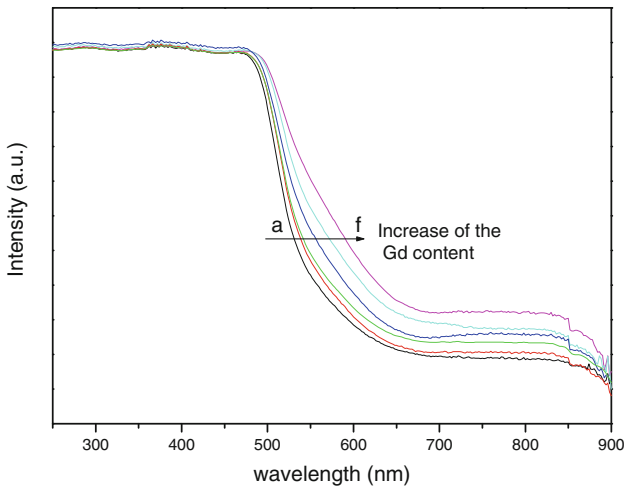

Fig. 5 The Kubelka–Munck transformed UV–vis diffuse reflectance spectra of different catalysts: (*a*) pure $BiVO_4$, (*b*) 0.28 wt%, (*c*) 0.71 wt%, (*d*) 1.22 wt%, (*e*) 2.93 wt%, and (*f*) 5.74 wt% of Gd in composite

$\ln(C_0/C_t) = kt + a$, where k, C_0, and C_t denote the apparent reaction rate constant, the initial concentration, and the concentration at the reaction time of t, respectively. As the concentration of MO has a linear relation with its absorbance, it can be approximated to $\ln(A_0/A_t) = kt + a$, which belong to the first order kinetics. This is confirmed by a approximate linear-plot of $\ln(C_0/C_t)$ with t as shown in Fig. 6. And from the plotted lines, the kinetic parameters of each catalyst can be calculated and listed in Table 1.

Effects of dopants on the enhanced photocatalytic activities

According to the standard redox potentials of E^{θ} (O_2/O_2^-) = +0.41 V, E^{θ} (Gd^{3+}/Gd) = −2.40 V [33], and E_{vb} ($BiVO_4$) = 1.21 V versus NHE [34], the presence of Gd^{3+} in the $BiVO_4$ may promote the electron transition in the semiconductor by the following electron-consuming reactions:

$$Gd^{3+} + 3e \rightarrow Gd \quad (1)$$

$$Gd + 3O_2 \rightarrow Gd^{3+} + 3O_2^- \quad (2)$$

It is generally believed that MO molecule can be excited under visible-light irradiation [35] and the excited state of MO molecule (MO*) can inject electrons into the conduction band (CB) of $BiVO_4$. The dye cationic radical ($MO^{\bullet+}$) produced after electron injection is less stable than the MO molecule in ground state, as a result, unstable

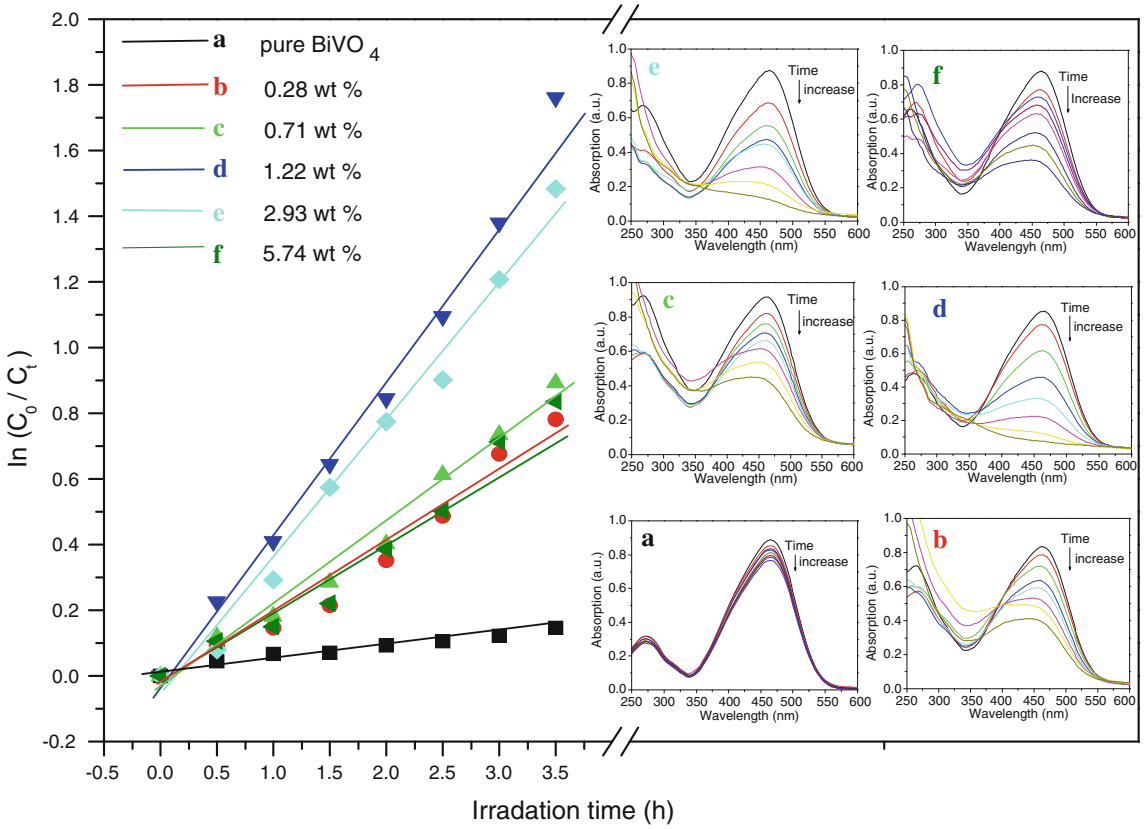

Fig. 6 Relationship between $\ln(C_0/C_t)$ and treatment time under visible-light irradiation. *Inset*: UV–vis spectra profile changes of photocatalytic degradation of 10 mg/L MO by different catalysts at different irradiation times

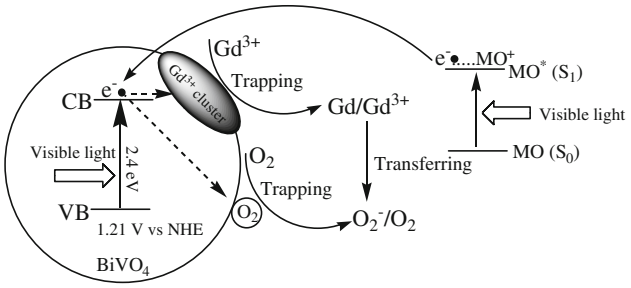

Scheme 1 Schematic photocatalytic mechanism of MO–Gd_2O_3/$BiVO_4$ composite under visible-light irradiation

$MO^{\bullet+}$ can be directly degraded into its products by reacting with super-oxidizing anionic radials or other active oxygen, such as $HO^{\bullet}$ or $O_2^{\bullet-}$ [10]. In the meantime, it is also extremely susceptible for the recombination between $MO^{\bullet+}$ and the electrons if the injection electrons accumulate in the CB of $BiVO_4$. So, the electrons trapping (Eq. 1) and electrons transferring (Eq. 2) reactions become two key steps to inhibit electron-$MO^{\bullet+}$ recombination. So, the gadolinium oxide loaded in $BiVO_4$ plays an important role in promoting the electron trapping and electron transferring significantly in the MO-Gd_2O_3/$BiVO_4$ system. The possible reaction mechanism in this system can be illustrated in Scheme 1.

Conclusion

Gd_2O_3/$BiVO_4$ composite catalysts were synthesized using hydrothermal method. The composite catalysts showed a structure of monoclinic-$BiVO_4$ type and dispersed particles with high crystallinity than the pure $BiVO_4$; they also exhibited enhanced photocatalytic activity when decomposed MO molecules in aqueous solution under visible-light irradiation. Besides the morphologies and structures changes of particles, the electron-scavenging effect by Gd^{3+}/Gd ion-pairs also contribute to the enhanced photocatalytic activities.

Acknowledgement We acknowledge the financial support from the General Program of Beijing Municipal Education Committee (No. KM200910009011).

References

1. Xiao GC, Wang XC, Li DZ, Fu XZ (2008) J Photochem Photobiol A 193:213
2. Yu JQ, Kudo A (2006) Adv Funct Mater 16:2163
3. Tücks A, Beck HP (2007) Dyes Pigm 72:163
4. Lee JS (2005) Catal Surv Asia 9:217
5. Zhou L, Wang WZ, Xu HL (2008) Cryst Growth Des 8:728
6. Gotic M, Music S, Ivanda M, Soufek M, Popovic S (2005) J Mol Struct 744–747:535
7. Xu H, Li H, Wu C, Chu J, Yan Y, Shu H (2008) Mater Sci Eng B 147:52
8. Guillodo M, Fouletier J, Dessemond L, Gallo PD (2001) J Eur Ceram Soc 21:2331
9. Kohtani S, Tomohiro M, Tokumura K, Nakagaki R (2005) Appl Catal B 58:265
10. Long M, Cai W, Cai J, Zhou B, Chai X, Wu Y (2006) J Phys Chem B 110:20211
11. Chatchai P, Murakami Y, Kishiokal S, Nosaka AY, Nosaka Y (2009) Electrochim Acta 54:1147
12. Xu H, Li H, Wu C, Chu J, Yan Y, Shu H, Gu Z (2008) J Hazard Mater 153:877
13. Jiang H, Endo H, Natori H, Nagai M, Kobayashi K (2009) Mater Res Bull 44:700
14. Ge L (2008) Mater Chem Phys 107:465
15. Ge L (2008) Mater Lett 62:926
16. Yang YL, Qiu L, Harrison WTA, Christoffersen R, Jacobson AJ (1997) J Mater Chem 7:243
17. Neves MC, Lehocky M, Soares R, Lapcik L, Trindade T (2003) Dyes Pigm 59:181
18. Yao W, Iwai H, Ye J (2008) Effects of molybdenum substitution on the photocatalytic behavior of $BiVO_4$. Dalton Trans 1426
19. Jiang H, Nagai M, Kobayashi K (2009) J Alloy Compd 24:821
20. Li L, Yan B (2008) J Alloy Compd 476:624
21. Xu H, Wu C, Li H, Chu J, Sun J, Xu Y, Yan Y (2009) Appl Surf Sci 256:597
22. El-Bahy ZM, Ismail AA, Mohamed RM (2009) J Hazard Mater 166:138
23. Xie Y, Yuan C, Li X (2005) Mater Sci Eng B 117:325
24. Zhang A, Zhang J, Cui N, Tie X, An Y, Li L (2009) J Mol Catal A 304:28
25. Sczancoski JC, Bomio MDR, Cavalcante LS, Joya MR, Pizani PS, Varela JA, Longo E, Li MS, Andres JA (2009) J Phys Chem C 113:5812
26. Kudo A, Omori K, Kato H (1999) J Am Chem Soc 121:11459
27. Uwamino Y, Ishizuka T (1984) J Electron Spectros Relat Phenomena 34:67
28. Ranjit KT, Willner I, Bossmann SH, Braun AM (2001) J Catal 204:305
29. Peng TY, Du PW, Hu B, Jiang ZC (2000) Anal Chim Acta 421:75
30. Zhao D, Peng T, Liu M, Lu L, Cai P (2008) Microporous Mesoporous Mater 114:166
31. Xu J, Ao Y, Fu D, Yuan C (2009) J Hazard Mater 164:762
32. Ollis DF (1985) Environ Sci Technol 19:480
33. Huheey JE (1983) Inorganic chemistry: principles of structure and reactivity, 3rd edn. Harper&Row, New York
34. Walsh A, Yan Y, Huda MN, Al-Jassim MM, Wei SH (2009) Chem Mater 21:547
35. Beveridge DL, Jaffe HH (1966) J Am Chem Soc 88:1948